Growth of Single-Crystalline Wurtzite Aluminum Nitride Nanotips with a Self-Selective Apex Angle**

By *Shih-Chen Shi*, *Chia-Fu Chen*, *Surojit Chattopadhyay*, *Zon-Huang Lan*, *Kuei-Hsien Chen*, and *Li-Chyong Chen**

Single-crystalline, hexagonal aluminum nitride nanotips are fabricated using a vapor-transport and condensation process (VTCP) on silicon substrates with or without a catalyst layer. The resultant tips have very sharp nanoscale apexes (~1 nm), while their bases and lengths are up to hundreds of nanometers wide and several micrometers long, respectively. It has been demonstrated that the thickness of the gold-catalyst layer plays a critical role in controlling the size of the tip; in addition, a catalyst-free growth mode has been observed, which results in lesser control over the nanotip morphology. Nevertheless, a remarkably narrow distribution of the apex angle of the nanotips, regardless of whether or not a catalyst was used in the VTCP, has been obtained. Compared with the commonly observed ridge and pyramid structures, the nanotips produced by VTCP have higher angles (~81°) between the tilted (221) and the basal (001) planes that encase it. A mechanism for this self-selective apex angle in aluminum nitride nanotip growth is proposed.

1. Introduction

The numerous important applications of the group-III nitrides, including InN, GaN, AlN, and their alloys, have attracted significant research interest over the last decade.[1–2] Among them, AlN has the highest bandgap of 6.2 eV, and a large exciton binding energy.[3] Potential applications in surface acoustic wave devices[4,5] and ultraviolet sensors[6] have already been demonstrated. Application in field-emission devices has also been suggested, because reported values of the electron affinity of AlN are rather small (~0.6 eV) or even negative.[7–9] The nanoscale group-III nitrides automatically qualify as ideal testing systems to study the reported changes in optoelectronic and electrical properties in low dimensions. Various strategies have been successfully developed for the fabrication of one-dimensional (1D) group-III nitride nanostructures, especially nanowires and nanorods. A comprehensive compilation of these results has been published recently.[10] GaN, as the center of attraction, saw the most rapid development[11]—in contrast to AlN, whose growth was relatively subdued and the routes for its synthesis were limited. Nevertheless, AlN nanowires, whiskers, and nanotubes have been obtained by chloride-assisted growth,[12,13] arc processes,[14] carbothermal reduction,[15,16] and gas-reduction–nitridation.[17] However, very recently, there has been an increased activity in this field with quite a few reports on nanowires, nanotubes, and nanobelts decorating the 1D AlN domain. Vapor–liquid–solid (VLS) growth of hexagonal AlN nanowires and nanotubes with [001] growth direction have been reported at temperatures above 1100 °C.[18,19] Hexagonal AlN nanobelts with a rectangular cross-section and a [001] growth direction also made their appearance.[20] A cubic-AlN nanotube with a boron nitride (BN) wrapping (AlN–BN composite nanotube) has been prepared at a temperature of 1200 °C, using a two-stage growth mechanism.[21] However, AlN nanotips with high aspect ratios, unlike the pyramids,[22] also form a special class in the 1D family, and have not been reported before.

Nanotips in Si-based and other more conventional semiconductor systems have been demonstrated and explored for various potential applications such as field emitters,[23–25] solar cells,[26] biological and chemical sensing devices,[27–29] as well as optical nanodevices.[30,31] Until now, optical lithography has played the major role in fabricating sharp tips, but these are limited to 50 nm in radius.[32–34] A novel electron cyclotron resonance plasma-assisted dry-etching technique has recently been developed for producing ultrafine tips (~1 nm) of a wide range of material systems, excluding AlN.[35] These tips (Si, poly-Si, GaN, GaP, and Al) can have apex diameters from 2 to 20 nm, and growth directions dependent on the orientation of the starting wafers. The approaches described above can be classified as top–down techniques and are most suitable for plate or wafer processes. In this study, we report on the first synthesis of single-crystalline AlN nanotips (AlNNTs) with a monodisperse angle distribution via simple VTCP, in both cata-

[*] Dr. L. C. Chen
Center for Condensed Matter Sciences
National Taiwan University
1 Roosevelt, Sec. 4, Taipei 106 (Taiwan)
E-mail: chenlc@ccms.ntu.edu.tw
S. C. Shi, Prof. C. F. Chen
Department of Materials Science and Engineering
National Chiao Tung University
1001 Ta Hsueh Road, Hsinchu 300 (Taiwan)
Dr. S. Chattopadhyay, Z. H. Lan, Dr. K. H. Chen
Institute of Atomic and Molecular Sciences
Academia Sinica
PO Box 23-166, Taipei 106 (Taiwan)

[**] The authors gratefully acknowledge the financial supports for this project from the National Science Council (NSC) and the Ministry of Education (MOE) in Taiwan. The authors also thank Prof. Guang-Yu Guo and Chung-Huai Chang in the Department of Physics, National Taiwan University, for technical support.

DOI: 10.1002/adfm.200400324

lytic and catalyst-free modes, at 950 °C. This temperature is significantly lower than that of the conventional carbothermal reduction and nitridation process for AlN. Gold-coated silicon substrates have been used to produce the AlNNTs, where the gold nanoparticulates formed at the high temperature acted as the nucleation sites for the AlNNTs growth. The morphology and crystal structure of AlNNTs were examined using high-resolution field-emission scanning electron microscopy (HRFE-SEM), transmission electron microscopy (TEM), X-ray diffractometry (XRD), and micro-Raman analysis. The structural evolution was monitored and a growth mechanism is proposed.

2. Results and Discussion

Pure aluminum powder and metal-coated (Au, Pt, Al) silicon substrates were placed in a ceramic boat inside a quartz tube, which was degassed, purged, and then heated to 950 °C in the presence of ammonia. After the reaction (~30 min), the system was cooled down to room temperature and the whitish product on the silicon substrate was collected. Figures 1a–c show typical SEM images of the morphologies of the as-grown AlNNTs on silicon substrates coated with an Au layer of various thicknesses. AlNNTs grown on a Au-coated (7 nm thick) Si substrate exhibited a mean diameter of 10 nm at the apex, 80 nm at the base, and 250 nm in length (Fig. 1a). AlNNTs grown with progressively thicker Au layers produced longer nanotips (300–3000 nm), with wider apex (20–100 nm) and base (100–700 nm) diameters (Figs. 1b,c). A typical cross-sectional SEM image of AlNNTs is shown in Figure 1d. This image displays a high density of quasi-aligned AlNNTs uniformly distributed over the entire substrate. The tip-like morphology suggests that the growth rate of the AlNNTs in the axial direction far outpaces the growth rate in the radial direction. Along with the AlNNTs, some non-nitrided metallic Al residue could be found at the base of the nanotips. The beauty of this VTCP technique lies in the size-control of the nanotips, which can be achieved simply by adjusting the thickness of the gold layer and keeping the other growth parameters, such as temperature and gas-flow rates, fixed. However, a number of other metals, such as aluminum (Fig. 2a) or platinum (Fig. 2b), can be used to produce the AlNNTs, since the eutectic temperatures of these metals with silicon lie below the reaction temperature of 950 °C. Furthermore, AlNNTs can even be grown on bare Si (without metal coating, Fig. 2c), but they exhibit relatively poor morphology, indicating that a metal coating is not indispensable for the growth, but it does help in controlling the morphology of the AlNNTs, and, perhaps, it increases the yield somewhat. But before coming to any such conclusion, a closer look at the initial stages of growth was deemed necessary.

The SEM images in Figures 3a–c demonstrate the initial growth of AlNNTs. The Al nanocrystals form within the first 15 min of growth and can be easily seen at the base of the AlNNTs (Fig. 3a). Figures 3b,c represent the morphology during the first 20 and 25 min of growth, respectively, with nanotip formation typically completed in 25 to 30 min. The corresponding elemental analysis by energy-dispersive X-ray spectroscopy (EDS) of the nanotip body and nanoparticles lying at the base of the nanotip is shown in Figure 3d. It is quite clear that the nanotip body showed a pronounced nitrogen component, whereas no Au signal could be obtained from the apex of such tips, marked A in Figure 3c; this fact excludes the possibility of a VLS growth mechanism. The crystallites lying at the base of the nanotips, marked B in Figure 3c, from which the nanotips evolved, yielded signals predominantly from Al, Au, and Si with no or little nitrogen component (Fig. 3d). The carbon and copper signals in Figure 3d come from the amorphous carbon-coated copper grids used for the TEM measurements. Two interesting inferences can be drawn from Figure 3d. First, the nanocrystal at the base is predominantly Al, and second, the Al at the tip is compounded with nitrogen. Both of these facts will be corroborated from the XRD results to be discussed later in the paper. However, the existence of the AlN phase in the nanotips is established conclusively from the TEM and XRD results. The presence of Au along with Al in the nucleating crystallites only indicates that either pure gold or a gold silicide phase may be controlling the nucleation and the smooth and finer morphology of the AlNNTs. In fact, the thickness of the Au layer is the key to the resultant morphology of the AlNNTs (Fig. 1). Au redundancy during growth resulted in larger crystallites with a corrugated morphology of the edges (Fig. 2c). The fact that AlNNTs can be grown on bare silicon (Fig. 2c) as well as on silicon covered with Al (Fig. 2a) indicates that a self-catalytic role of pure Al nanocrystals cannot be ruled out. Al vapor condenses as crystalline Al on the catalytic gold or the gold silicide sites, and we believe that these crystallized Al

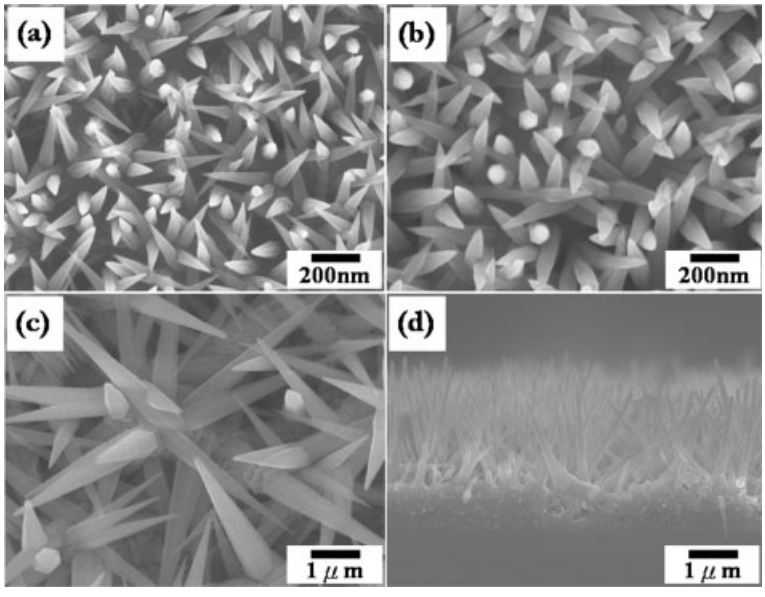

Figure 1. Typical SEM images of the AlN nanotips grown with an Au layer of a) 7 nm, b) 15 nm, and c) 50 nm thickness on Si. d) Typical cross-sectional SEM image of AlN nanotips grown with a Au-coated (15 nm) Si substrate.

ADVANCED FUNCTIONAL MATERIALS

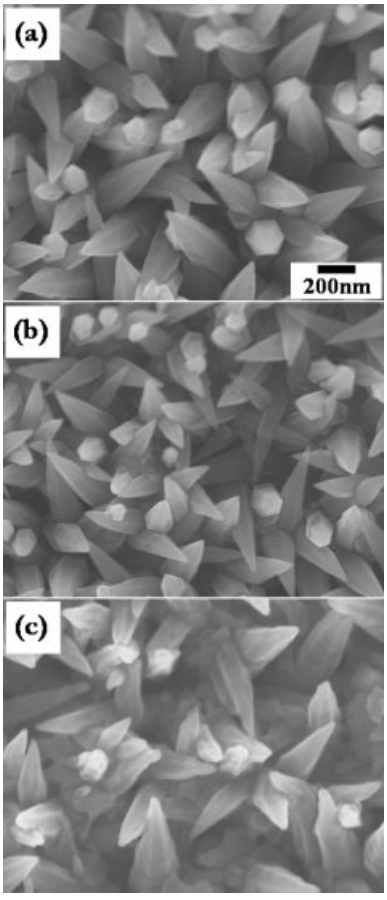

Figure 2. SEM images of AlN nanotips grown with a) Al, 15 nm, b) Pt, 15 nm, and c) no metal coating on the Si substrate.

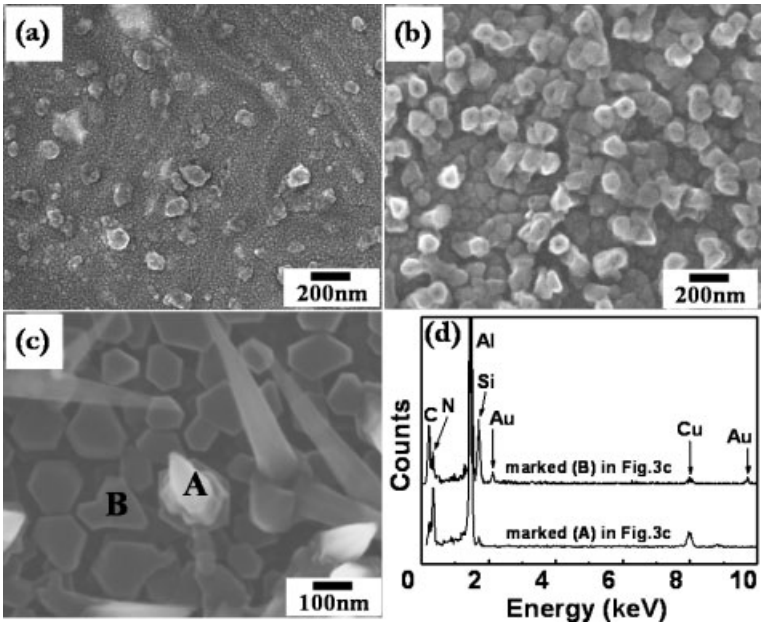

Figure 3. SEM images of AlN nanotips grown with Au (15 nm on Si) for a) 15 min, b) 20 min, and c) 25 min. d) The corresponding TEM–EDS spectra of the AlN nanotip and nanoparticle marked A and B, respectively, in (c).

nanoparticles, present at the bases of the AlNNTs, served as the nucleation sites for AlNNT growth following deposition of reacted Al and N vapors.

In order to investigate the structural evolution of the AlNNTs, XRD analyses were performed at various stages of growth. As shown in Figure 4a, the XRD data for the initial stage shows the presence of Al only, whereas the corresponding data for the later stage shows a number of relatively sharp diffraction peaks that can be indexed to a hexagonal structure with lattice constants a of 0.311 nm and c of 0.498 nm, which is consistent with the standard value for bulk hexagonal AlN (Joint Committee for Powder Diffraction Standards, JCPDS, Card No. 25-1133). While the signals from Au are negligible, the Al signals remain detectable in the XRD spectra. Presumably the signals are due to the unreacted aluminum, which can crystallize on the Au particles at the base of the AlNNTs during the initial high-temperature processing of the reactants. It should be noted that all samples showed similar XRD patterns, indicating that the structure of the nanotips is reproducible under all deposition conditions used. This reproducibility is a prerequisite for any synthetic technique to become accepted.

Raman spectra of the AlNNTs were obtained at room temperature (Fig. 4b) to further the knowledge of its structure. In the spectrum shown, distinct first-order modes of the peaks corresponding to the A_1 (TO), E_2 (high), E_1 (TO), and A_1 (LO) modes at around 609.4, 653, 668, and 894 cm^{-1}, respectively, were observed. These Raman peaks are signatures for wurtzite AlN as reported previously for bulk, thin-film, nanowire, and nanobelt structures.[18,20,36,37] However, these peak positions were given alternative assignments in an earlier work.[38] These Raman peaks were not detected in the samples containing predominantly nanocrystals (such as those grown for 15 min or less as shown in Fig. 3a), suggesting that the AlN signals indeed originate from the well-crystallized tips.

High-resolution TEM (HRTEM), along with selected-area electron diffraction (SAED), was employed to further analyze the structure and crystallographic orientations of these AlNNTs. All nanotips appear to be homogeneous without any grain boundaries, indicating the single-crystalline nature of each individual AlNNT. As shown in Figure 5b, the HRTEM image of the apex reveals lattice spacings of 0.497 and 0.269 nm (in parallel and normal to the axial direction), which are in good agreement with the d_{001} and $d_{1\bar{1}0}$ spacings of h-AlN, respectively. In agreement with the SAED pattern, the direction of the AlNNTs was found to be [001] along the long axis (inset, Fig. 5b). AlN whiskers growing along $\{10\bar{1}0\}$ and $\{\bar{1}2\bar{1}0\}$ close-packed planes have already been reported,[39] and a [001] growth direction of some 1D nanostructures was also observed.[19,20] HRTEM examination and SAED performed over several nanotips made from gold films of different thicknesses, and also at different locations on each nanotip, yielded similar diffraction patterns. Elemental analysis of a single AlNNT body (shown in

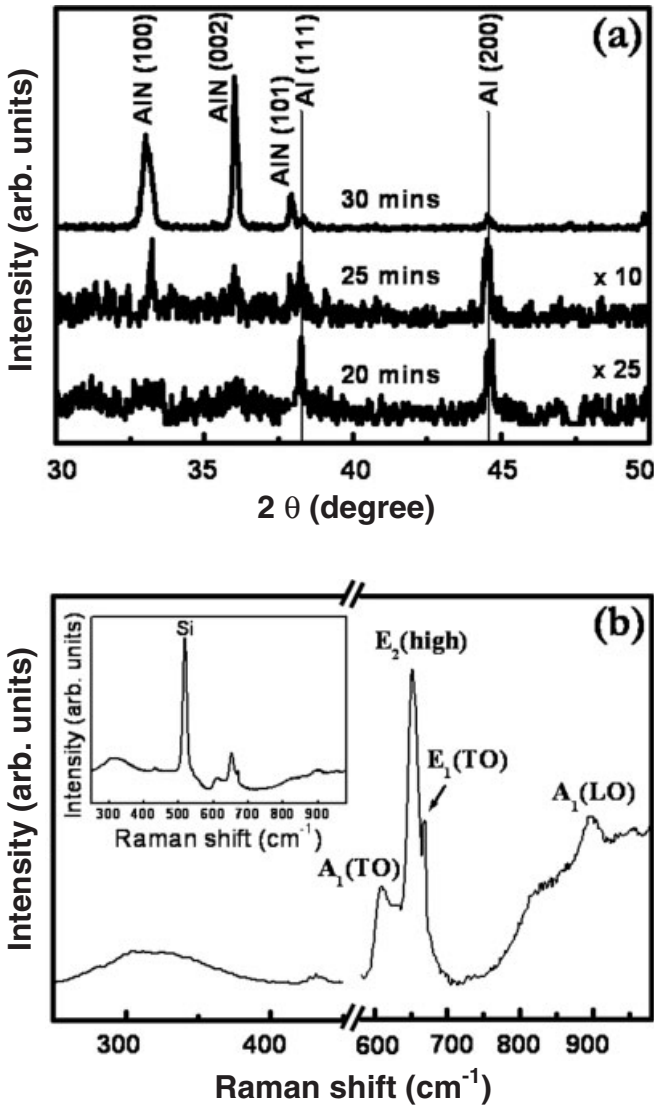

Figure 4. a) Typical XRD spectra taken at three different stages of growth. The initial stage shows only Al signals and the corresponding one with fully grown nanotips shows two crystalline phases of Al and hexagonal AlN. b) Raman spectrum, with a discontinuous abscissa, of the AlN nanotips on silicon substrate. Inset shows a continuous Raman spectrum of the AlN nanotips with the silicon signal included. All the XRD and Raman spectra were measured from samples prepared on 15 nm Au coated Si substrate.

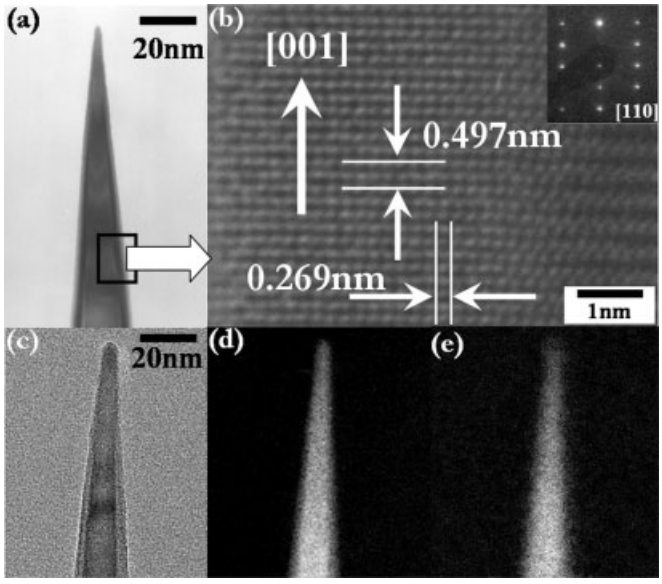

Figure 5. a) TEM image of an AlN nanotip and b) HRTEM image of a single AlN nanotip with clear lattice images. The inset shows a SAED pattern of the nanotip, indicating the single-crystalline nature with [110] zone axis and the growth direction along [001]. c) TEM image of a single AlN nanotip with corresponding Al (d), and N (e) mapping using EELS.

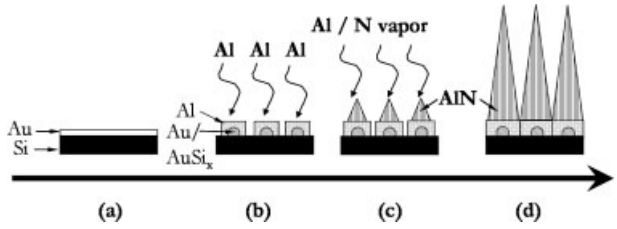

Figure 6. Schematic diagram of the growth mechanism of AlN nanotips. a) Au layer coated on the Si substrate. b) Gold or gold silicide nanoparticles form as the nucleation sites for the subsequent aluminum deposition. c) Al and N are absorbed on the nucleation sites bringing about the initial growth of AlN nanotips. d) AlN nanotips elongate with time when the reaction temperature is kept at 950 °C.

Fig. 5c) by electron energy-loss spectroscopy (EELS) clearly established a stoichiometric AlN composition with Al (Fig. 5d) and N (Fig. 5e) mapped with a similar rate of occurrence.

Based on the above results, a complete growth mechanism of AlNNTs can be proposed, a schematic description of which is given in Figure 6. As the reaction temperature was ramped up from room temperature to 950 °C, droplets of catalyst metals (Au, Pt) or their respective silicide phases will be formed in the vicinity of their respective eutectic temperatures. In the case of uncoated Si, the self-catalytic Al or Al-alloy droplets, possibly Al–Si, are believed to be the nucleation sites. Al vapors, generated above 660 °C, dissolve in these droplets, supersaturating them and finally resulting in the expulsion of elemental Al as nanocrystals. Fully reacted vapors of Al and N deposit as stoichiometric AlN on the Al base, where a rapid growth along the axial direction [001] and an inhibited growth along an orthogonal (radial) direction was observed, giving rise to the tip shape. Physically speaking, we can visualize this as a pyramid of growth consisting of two-dimensional (2D) islands growing on top of each other. The tilted face of the nanotip can be considered as a vicinal face consisting of a train of parallel steps with mono- or polyatomic step heights (h). The high slope (81° in our case) of this vicinal face is determined by the high rate of 2D nucleation and step propagation, which results in a small step spacing (λ) and high step density ($p = h/\lambda$).[40] A lower rate of 2D nucleation and step propagation will result in a pyramid with much smaller slope of the tilted face. During initial growth, the diffusion length of the pure, non-nitrided Al atom, expelled from the catalyst or arriving fresh from the gas phase, was high, resulting in the formation of larger 2D Al nanocrys-

tals at the base of the nanotips and a significant step spacing. Additional Al atoms impinging on the growth surface will nucleate 2D AlN islands more efficiently as it reacts with ammonia-dissociation products (NH_x). Then it will diffuse as AlN molecules on the growth surface, producing the closely spaced mono- or polyatomic steps discussed earlier. This diffusion is a function of the growth temperature and the ratio of group-V to group-III atoms.[41] This argument is supported by our observation that an increased growth temperature, and hence increased diffusion length, resulted in the formation of AlN nanorods instead of nanotips, which will be reported separately. The rate of 2D AlN island nucleation and the diffusion length of the precursors are a function of growth temperature and vapor supersaturation and are believed to be key in controlling the morphology of the 1D nanomaterials. The growth inhibition along the radial direction is possible via passivation of the dangling bonds on that surface by, possibly, oxygen.

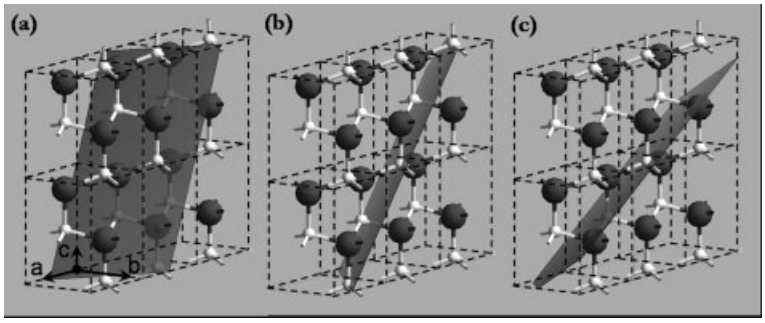

Figure 7. Atomic arrangement in an AlN crystal showing the stable non-growth surfaces of a) (221), b) (1$\bar{1}$1), and c) (1$\bar{1}$2) making angles of 81°, 61°, and 43°, respectively, with the basal plane. The *c*-axis shown in the figure is the [001] direction.

As was mentioned in a review by Felice et al.,[39] the aluminum side of AlN can bond to the silicon side of SiC(001), whereas the nitrogen face prefers the carbon side. In our case, the basal (001) plane is the Al-terminated surface having the higher growth rate. According to the Gibbs' free energy (ΔG) for the formation of Al–Al and Al–N at 950 °C, which is 120 and –94.5 kJ mol^{-1}, respectively, the Al-terminated surface offered the preferred growth surface for the incident Al–N, bonding to the nitrogen side. However, note that ΔG for Al–Al and Al–N at 660 °C (melting point of Al) is nearly identical at 2.97 and –6.85 kJ mol^{-1}, respectively, and the formation of Al nanocrystals cannot be inhibited. By the etching of AlN single crystals,[42] it was found that the angle between the basal plane and tilted plane of the AlN pyramid was about 61.6°, which is close to the angle between the (001) and (1$\bar{1}$1) planes in AlN. The (1$\bar{1}$1) planes are energetically stable, because of a smaller number of bonds cutting through these planes. The energetically stable surface was exposed after etching was complete. In the case of an epitaxial AlN thin film on a SiC substrate, there exists a stable plane (namely (1$\bar{1}$2)) with a 43° angle with respect to the basal plane.[22] However, in our case, the angle between basal plane and tilted plane of the nanotip is much higher, roughly 81.5°, corresponding to the angle between the basal planes (001) and (221). It is thus suggested that these AlN nanotips are bound by (221) planes, which are non-growth surfaces, having fewer dangling bonds and hence being non-reactive, and the (001) basal plane provides the growth surface. Figure 7a shows the atomic arrangements in an AlN crystal with the non-growth planes (221) observed in the present work as well as (1$\bar{1}$1)[42] and (1$\bar{1}$2)[22] (Figs. 7b,c) reported previously. The similar dangling-bond environments in each of these cases can be used to rationalize the existence of the stable higher-index plane observed in the AlN nanotips. A similar basis for the facet formation in a GaAs ridge morphology has recently been reported.[43] The (221) planes can be H or N terminated, depending on the bond enthalpies of Al–H and Al–N, where the former is smaller. The rapid etching rate on the N-terminated surface may lead to dangling-bond passivation by H, which is formed by decomposition of the ammonia gas at 950 °C. However, at such high reaction temperatures, the stability of Al–H is questionable. In general, a high growth rate along the (001) basal plane with the stable (221) tilted surface generates the shape of the AlNNTs. Clearly the nanotips, with higher aspect ratios and tilted high-index planes, are different morphological species than the pyramids or the ridges observed earlier.

3. Conclusion

The growth of aluminum nitride nanotips on metal (Au, Al, and Pt)-coated, or even uncoated silicon substrates via a vapor-transport and condensation process has been demonstrated. A pure metal or metal silicide phase acts as the nucleation site for the precipitation of crystalline aluminum seeds for the aluminum nitride nanotip growth. For aluminum nitride nanotip growth on bare silicon, a self-catalytic activity of aluminum itself or its silicide phase was visualized. The resultant AlN nanotips exhibit a monodisperse distribution of apex angles. Transmission electron microscopy and X-ray diffraction studies suggest that these tips have hexagonal crystal symmetry with a preferred growth direction of [001] along the long axis and a stable (221) plane as the tilted surface.

4. Experimental

The AlNNTs were grown by a vapor-transport and condensation process using silicon substrates covered with gold, aluminum, or platinum which acted as catalysts. An aluminum oxide boat, carrying the metal-coated silicon substrate and some pure aluminum powder (SHOWA, Japan), was placed inside a quartz tube (25.4 mm in diameter). The Al powder was kept upstream and the Au-coated Si substrate was placed upside down (Au-coated side facing the Al powder) and downstream with respect to the flow of the nitriding gas, in this case NH_3. The quartz tube was housed in a conventional tube furnace. The quartz tube was degassed and then purged with ammonia NH_3 (30 sccm, sccm: standard cubic centimeters per minute), the atomic-nitrogen precursor. During the growth process, the furnace temperature was ramped up to 950 °C and held at that temperature for 30 min with an ammonia flow rate of 30 sccm. After cooling, the products collected on the silicon substrate were characterized using HRSEM (JEOL JSM6700F), and the structure of the nanotips was studied by HRTEM

using a JEOL JEM-4000EX instrument and by XRD using a Rigaku D/max system with Cu Kα radiation of 0.15418 nm. Micro-Raman spectra were obtained with a Renishaw system 2000 spectrometer with an Nd-YAG laser (excitation wavelength 532.2 nm).

Received: July 19, 2004
Final version: December 3, 2004

[1] S. Nakamura, G. Fasol, *The Blue Laser Diode*, Springer-Verlag, New York **1997**.
[2] J. H. Edgar, S. Strite, I. Akasaki, H. Amano, C. Wetzel, *Processing and Applications of Gallium Nitride and Related Semiconductors*, *Part A*, INSPEC, London **1999**.
[3] F. Davis, *Proc. IEEE* **1991**, *79*, 702.
[4] Y. Takagaki, P. V. Santos, E. Wiebicke, O. Brandt, H. P. Schonherr, K. H. Ploog, *Phys. Rev. B* **2002**, *66*, 155 439.
[5] V. Mortet, O. Elmazria, M. Nesladek, M. B. Assouar, G. Vanhoyland, J. D'Haen, M. D'Olieslaeger, P. Alnot, *Appl. Phys. Lett.* **2002**, *81*, 1720.
[6] L. Trinkler, L. Botter-Jensen, B. Berzina, *Radiat. Prot. Dosim.* **2002**, *100*, 313.
[7] V. M. Bermudez, T. M. Jung, K. Doverspike, A. E. Wickenden, *J. Appl. Phys.* **1996**, *79*, 110.
[8] A. T. Sowers, J. A. Christman, M. D. Bremser, B. L. Ward, R. F. Davis, R. J. Nemanich, *Appl. Phys. Lett.* **1997**, *71*, 2289.
[9] M. Kasu, N. Kobayashi, *Appl. Phys. Lett.* **2000**, *76*, 2910.
[10] L. C. Chen, K. H. Chen, C. C. Chen, in *Nanowires and Nanobelts—Materials, Properties and Devices*, Vol. 1 (Ed: Z. L. Wang), Kluwer, Dordrecht, The Netherlands **2003**, Ch. 9.
[11] C. C. Chen, C. C. Yeh, C. H. Chen, M. Y. Yu, H. L. Liu, J. J. Wu, K. H. Chen, L. C. Chen, J. Y. Peng, Y. F. Chen, *J. Am. Chem. Soc.* **2001**, *123*, 2791.
[12] J. A. Haber, P. C. Gibbons, W. E. Buhro, *Chem. Mater.* **1998**, *10*, 4062.
[13] K. J. Lee, D. H. Ahn, Y. S. Kim, *J. Am. Ceram. Soc.* **2000**, *83*, 1117.
[14] V. N. Tondare, C. Balasubramanian, S. V. Shende, D. S. Joag, V. P. Godbole, S. V. Bhoraskar, M. Bhadbhade, *Appl. Phys. Lett.* **2002**, *80*, 4813.
[15] R. L. Fu, H. P. Zhou, L. Chen, Y. Wu, *Mater. Sci. Eng. A* **1999**, *266*, 44.
[16] Y. J. Zhang, J. Liu, R. R. He, Q. Zhang, X. Z. Zhang, J. Zhu, *Chem. Mater.* **2001**, *13*, 3899.
[17] T. Suehiro, J. Tatami, T. Meguro, K. Komeya, S. Matsuo, *J. Am. Ceram. Soc.* **2002**, *85*, 715.
[18] Q. Wu, Z. Hu, X. Z. Wang, Y. N. Lu, K. F. Huo, S. Z. Deng, N. S. Xu, B. Shen, R. Zhang, Y. Chen, *J. Mater. Chem.* **2003**, *13*, 2024.
[19] Q. Wu, Z. Hu, X. Z. Wang, Y. N. Lu, X. Chen, H. Xu, Y. Chen, *J. Am. Chem. Soc.* **2003**, *125*, 10 176.
[20] Q. Wu, Z. Hu, X. Z. Wang, Y. Chen, Y. N. Lu, *J. Phys. Chem. B* **2003**, *107*, 9726.
[21] L. W. Yin, Y. Bando, Y. C. Zhu, D. Goldberg, M. S. Li, *Adv. Mater.* **2004**, *16*, 929.
[22] Y. Wu, A. Hanlon, J. F. Kaeding, R. Sharma, P. T. Fini, S. Nakamura, J. S. Speck, *Appl. Phys. Lett.* **2004**, *84*, 912.
[23] G. Y. Zhang, X. Jiang, E. Wang, *Science* **2003**, *300*, 472.
[24] C. L. Tsai, C. F. Chen, C. L. Lin, *Appl. Phys. Lett.* **2002**, *80*, 1821.
[25] H. C. Lo, D. Das, J. S. Hwang, K. H. Chen, C. H. Hsu, C. F. Chen, L. C. Chen, *Appl. Phys. Lett.* **2003**, *83*, 1420.
[26] C. C. Striemer, P. M. Fauchet, *Appl. Phys. Lett.* **2002**, *81*, 2980.
[27] J. J. Hickman, D. Ofer, P. E. Laibinis, G. M. Whitesides, M. S. Wrighton, *Science* **1991**, *252*, 688.
[28] V. S. Y. Lin, K. Motesharei, K. P. S. Dancil, M. J. Sailor, M. R. Ghadiri, *Science* **1997**, *278*, 840.
[29] D. Kovalev, V. Y. Timoshenko, N. Kunzner, E. Gross, F. Koch, *Phys. Rev. Lett.* **2001**, *87*, 68 301.
[30] W. I. Park, G. C. Yi, M. Kim, S. J. Pennycook, *Adv. Mater.* **2002**, *14*, 1841.
[31] F. A. Ponce, D. P. Bour, *Nature* **1997**, *386*, 351.
[32] C. C. Williams, R. C. Davis, P. Neuzil, *US Patent 5 969* 345, **1999**.
[33] F. G. Tarntair, L. C. Chen, S. L. Wei, W. K. Hong, K. H. Chen, H. C. Cheng, *J. Vac. Sci. Technol. B* **2000**, *18*, 1207.
[34] P. D. Kichambare, F. G. Tarntair, L. C. Chen, K. H. Chen, H. C. Cheng, *J. Vac. Sci. Technol. B* **2000**, *18*, 2722.
[35] C. H. Hsu, H. C. Lo, C. F. Chen, C. T. Wu, J. S. Hwang, D. Das, J. Tsai, L. C. Chen, K. H. Chen, *Nano Lett.* **2004**, *4*, 471.
[36] M. Kuball, J. M. Hayes, A. D. Prins, N. W. A. van Uden, D. J. Dunstan, Y. Shi, J. H. Edgar, *Appl. Phys. Lett.* **2001**, *78*, 724.
[37] T. Prokofyeva, M. Seon, J. Vanbuskirk, M. Holtz, S. A. Nikishin, N. N. Faleev, H. Temkin, S. Zollner, *Phys. Rev. B* **2001**, *63*, 125 313.
[38] C. Carlone, K. M. Lakin, H. R. Shanks, *J. Appl. Phys.* **1984**, *55*, 4010.
[39] R. D. Felice, J. E. Northrup, J. Neugebauer, *Phys. Rev. B* **1996**, *54*, R17 351.
[40] I. V. Markov, in *Crystal Growth for Beginners*, World Scientific, Singapore, Japan **1995**, Ch. 3.
[41] A. M. S. El Ahl, M. He, P. Z. Zhou, G. L. Harris, L. Salamanca-Riba, F. Felt, H. C. Shaw, A. Sharma, M. Jah, D. Lakins, T. Steiner, S. N. Mohammad, *J. Appl. Phys.* **2003**, *94*, 7749.
[42] D. Zhuang, J. H. Edgar, L. H. Liu, B. Liu, L. Walker, *MRS Internet J. Nitride Semicond. Res.* **2004**, *7*, 1.
[43] R. S. Williams, M. J. Ashwin, T. S. Jones, J. N. Neave, *J. Appl. Phys.* **2004**, *95*, 6112.

